

# Imaging interfacial micro- and nano-bubbles by scanning transmission soft X-ray microscopy

Lijuan Zhang,<sup>a\*</sup> Binyu Zhao,<sup>a</sup> Lian Xue,<sup>a</sup> Zhi Guo,<sup>a</sup> Yaming Dong,<sup>b</sup> Haiping Fang,<sup>a</sup> Renzhong Tai<sup>a\*</sup> and Jun Hu<sup>a\*</sup>

<sup>a</sup>Shanghai Institute of Applied Physics, Chinese Academy of Sciences, Shanghai 201204, People's Republic of China, and <sup>b</sup>Life and Environment Science College, Shanghai Normal University, Shanghai 200234, People's Republic of China. E-mail: zhanglijuan@sinap.ac.cn, tairenzhong@sinap.ac.cn, hujun@sinap.ac.cn

Synchrotron-based scanning transmission soft X-ray microscopy (STXM) with nanometer resolution was used to investigate the existence and behavior of interfacial gas nanobubbles confined between two silicon nitride windows. The observed nanobubbles of SF<sub>6</sub> and Ne with diameters smaller than 2.5 μm were quite stable. However, larger bubbles became unstable and grew during the soft X-ray imaging, indicating that stable nanobubbles may have a length scale, which is consistent with a previous report using atomic force microscopy [Zhang *et al.* (2010), *Soft Matter*, **6**, 4515–4519]. Here, it is shown that STXM is a promising technique for studying the aggregation of gases near the solid/water interfaces at the nanometer scale.

**Keywords:** interfacial science; nanobubbles; scanning transmission soft X-ray microscopy.

## 1. Introduction

Gas bubbles adsorbed at a liquid/solid interface is a classical phenomenon and plays an important role in many important physical, chemical and biological processes (Wallqvist & Berne, 1995; Huang *et al.*, 2003; ten Wolde & Chandler, 2002; Liu *et al.*, 2005; Ball, 2012). Recently, nanoscopic gas bubbles with heights of less than 100 nm but lateral sizes from several tens of nanometers to the micrometer scale have been found to exist at various surfaces immersed in water with a lifetime of hours and even days (Ohgaki *et al.*, 2010; Zhang *et al.*, 2007a, 2008a; Brenner & Lohse, 2008; Ducker, 2009; Seddon *et al.*, 2011). The astonishing stability of these nanobubbles contradicts classical thermodynamics. According to the Young–Laplace equation, such nanobubbles should not exist at all, since their small radius of curvature implies a high Laplace pressure inside the bubbles causing them to dissolve almost instantly (Simonsen *et al.*, 2004; Borkent *et al.*, 2010; Holmberg *et al.*, 2003; Ljunggren & Eriksson, 1997). For micrometer- or nanometer-sized bubbles, classical theory predicts that they should disappear within tens of milliseconds or less (Ljunggren & Eriksson, 1997). Nanobubbles with such a long lifetime are very important, not only because they pose a number of challenges to our conventional understanding of gas behaviors at interfaces but also because they are expected to have potential applications in many fields such as protein folding, stability of colloids and emulsions, and boundary slip in flowing water, *etc.* (Nguyen *et al.*, 2004; Vinogradova, 1995; Priezjev *et al.*, 2005).

Despite the theoretical problems, during the last ten years experiments on nanobubbles have focused on their existence and stability. After Parker *et al.* firstly proposed the nanobubbles concept in 1994 based on the force measurements between two solid plates immersed in liquid water (Parker *et al.*, 1994), many techniques have been employed to investigate the mysterious behavior of interfacial nanobubbles including attenuated total reflection infrared spectroscopy (Zhang *et al.*, 2007a), quartz crystal microbalance (Seo *et al.*, 2007; Zhang, 2008), neutron reflectometry (Steitz *et al.*, 2003) and X-ray reflectivity (Mezger *et al.*, 2006). However, all of these techniques only measure the thickness of a gassy layer at the near-wall region at solid/liquid interfaces, typically a spatial average of many hundred square micrometers. Therefore, these techniques cannot distinguish between the distributed individual nanobubbles on the surface and a uniform gassy layer trapped between substrate and liquid. Since the distribution of the nanobubbles on a surface has been difficult to control in current experiments, the thicknesses of the gassy layer measured by those techniques usually varied quite a lot. If the density of the nanobubbles was too low, the gassy layer would not be detected, which has led to arguments about whether the nanobubbles indeed existed at all (Evans *et al.*, 2004; Seo & Satija, 2006; Doshi *et al.*, 2005).

Major progress was made by introducing high-resolution imaging techniques. Individual nanobubbles were first imaged by atomic force microscopy (AFM) in tapping mode (Lou *et al.*, 2000; Ishida *et al.*, 2000), whereby an immersed probe is rapidly tapped against a solid surface. AFM imaging proved

the existence of individual nanobubbles with a lifetime as long as hours or even days. Moreover, AFM revealed detailed structures of the nanobubbles, and new nanoscopic gas morphology such as pancakes and multiple layers have also been discovered (Zhang *et al.*, 2007b, 2008b, 2009; Seddon *et al.*, 2010; Seddon & Zandvliet, 2010). Importantly, it is easy to provide a quantitative surface distribution of nanobubbles by simply counting their numbers on the surface per unit square in the AFM images. By comparing the density of nanobubbles prepared with and without degassing, it could clearly be shown that the observed nanobubbles were truly caused by dissolved gases, finally convincing many critics (Zhang *et al.*, 2004, 2006; Hui *et al.*, 2009; Craig, 2011; Guan *et al.*, 2012; Guo *et al.*, 2012). However, AFM imaging is intrusive and it has been questioned whether an AFM tip could actually lead to the breakdown of a uniform gassy layer into nanobubbles. We could not tell whether the nanobubbles we observed were previously existing nanobubbles or just a result of being induced by the AFM tip. Also, one can imagine that if the nanobubbles on some surfaces are not sufficiently stable they would disappear after being disturbed by the AFM tip and would not be detected. In order to further explore the behavior of nanobubbles, there has been a call for new imaging techniques which have a high spatial resolution and are non-intrusive. Recently, optical interference-enhanced reflection microscopy and scanning transmission electron microscopy (STEM) have been used to image nanobubbles on surfaces (Karpitschka *et al.*, 2012; White *et al.*, 2011). Even though the spatial resolution of optical interference-enhanced reflection microscopy is limited to  $\sim 300$  nm, and for STEM the sample preparation is usually quite difficult and the strong electron beams in STEM may have some unexpected influence on the behavior of nanobubbles, much useful information has been obtained (Karpitschka *et al.*, 2012; White *et al.*, 2011).

The X-ray absorption-based technique is a typical non-intrusive measurement which has long been widely used in many scientific fields. During recent years, with the development of synchrotron radiation techniques, zone-plate-based scanning transmission soft X-ray microscopy (STXM) has become a unique analysis tool which takes advantage of

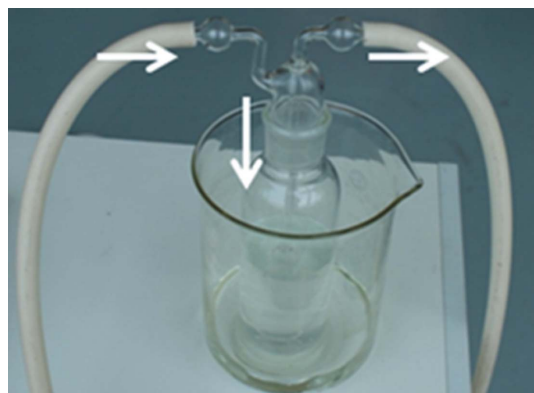


**Figure 1**  
Set-up of the gas injecting system. The white arrows indicate the directions of gas flow. The volume of the multi-porous washing bottle is 500 ml.

elemental absorption contrast to image samples down to about 15 nm (Chao *et al.*, 2005). In principle, the non-intrusive measurement, nanoscopic spatial resolution and chemical sensitivity makes STXM an ideal technique for studying the properties and behavior of individual nanobubbles at interfaces.

In this paper we show that STXM with nanometer resolution could be used to image nanobubbles with gas contents of SF<sub>6</sub> and Ne between two silicon nitride windows in water solutions. The stability of these nanobubbles with different length scales was investigated when exposed to soft X-ray irradiation.

## 2. Experimental

### 2.1. Materials

Water with a conductivity of 18.2 MΩ cm was obtained from a Milli-Q system (Millipore Corp., Boston, MA, USA). Urea (<99.5%), α-cyclodextrin (α-CD, 99.5%) and carbon porous microspheres (<500 nm) were purchased from Sigma and used without further purification. Silicon nitride (Si<sub>3</sub>N<sub>4</sub>) windows (dimensions 5 mm × 5 mm, window 1.5 mm × 1.5 mm × 100 nm, SN-LDE-510-15, Shanghai NTI, China) served as the substrates for the nanobubbles.

### 2.2. Preparation of nanobubbles

Preparation of the nanobubbles was performed as follows. First, millipore water was degassed for  $\sim 2$  h at a pressure of 0.1 atm in a desiccator. Urea, α-CD or carbon microspheres were added to the degassed water to obtain the solutions (4.5–5.0 mg ml<sup>-1</sup>). Then SF<sub>6</sub> gas (purity 99.9999%, from Wonik Materials) or Ne (purity 99.999%, from Shanghai Shenkai Gas) was injected into these solutions for  $\sim 30$  min in a washing bottle. The set-up is shown in Fig. 1. At first, one droplet of the gas solution (about 3.0 μl) was deposited onto the surface of one Si<sub>3</sub>N<sub>4</sub> window. Then another Si<sub>3</sub>N<sub>4</sub> window was carefully put on top of this droplet. Vacuum glue (two components, from Agilent) was used to seal these two Si<sub>3</sub>N<sub>4</sub> windows. After  $\sim 1.5$  h for the glue to solidify, the sample was loaded into the sample holder in the experimental chamber. Reference experiments were performed at the same time. The degassed systems before and after gas injection were measured.

### 2.3. STXM imaging

The samples were investigated using the newly constructed BL08U1A STXM beamline at the Shanghai Synchrotron Radiation Facility (SSRF), a 3.5 GeV third-generation synchrotron source. The detailed principle of STXM and the design of the microscope have been described elsewhere (Xue *et al.*, 2010). As shown in Fig. 2, the monochromatic X-ray beam was focused using a Fresnel zone plate to a 30 nm spot (this work) on the sample. The sample was raster scanned with synchronized detection of transmitted X-rays to generate the images. The sample was imaged in transmission mode in helium (He,  $\geq 99.999\%$ , Shanghai Chunyu Special Gas) at

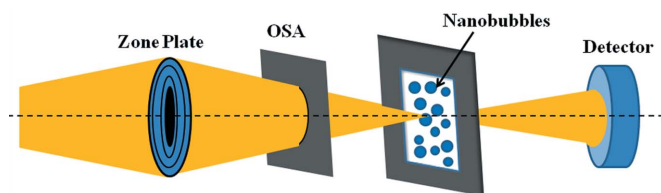


**Figure 2**  
Schematic of the configuration of zone-plate-based STXM.

pressure (300–500 torr). The transmitted photon flux was measured using a photomultiplier tube (Hamamatsu, Japan). A 800 lines  $\text{mm}^{-1}$  grating and 50  $\mu\text{m}$  exit slit were used for F or Ne *K*-edge imaging and spectroscopy, providing an energy resolution of 6000/700 eV ( $E/\Delta E$ ). Images were recorded at selected energies through the F 1s region (680–720 eV) or Ne 1s region (860–910 eV). The photon energy was calibrated by measuring pure  $\text{SF}_6$  or Ne in the experimental chamber at a pressure of  $\sim 3$ –10 torr.

### 3. Results and discussions

The preparation of nanobubbles in the STXM experiments was quite different from that in the AFM experiments where large amounts of nanobubbles could be produced by solution-exchanging or electrochemical methods (Lou *et al.*, 2000; Zhang *et al.*, 2006; Hui *et al.*, 2009). Those methods are difficult to perform in a very small space in which the volume of the water solution needed in STXM is only about 2–3  $\mu\text{l}$ . The space between two silicon nitride membranes was controlled by the thickness of the water layer between them. It was shown that a water solution thickness of less than 500 nm is the best thickness for obtaining good contrast from samples. Thus it was difficult to perform solution-exchanging in the STXM sample cell. On the other hand, directly immersing the solid surface in gas-saturated water usually led to fewer nanobubbles. Therefore, in order to bring more gas into the water, we added small amphiphilic water-soluble organic molecules, such as  $\alpha$ -CD and urea as used by Jin *et al.* (2007), to stabilize the nanobubbles and prevent coalescence. Moreover, carbon microporous particles were also used in this experiment for comparison. Meanwhile, the pressure was kept to 300–500 torr to prevent the evaporation of water in the chamber when performing the STXM experiments.

The types of gases used were very crucial to the STXM experiments. We chose  $\text{SF}_6$  and Ne as the main gases for studying the nanobubbles.  $\text{SF}_6$  has a large absorption coefficient at the F *K*-edge. The F and Ne *K*-edges are both in the energy range of soft X-rays (250–2000 eV, SSRF). Importantly, these two energies of Ne and F absorption are easy to recognize and distinguish from the absorptions of other elements, such as oxygen, nitrogen and carbon which generally exist on the solid surfaces or in water solution.

Figs. 3(a) and 3(b) show Ne and  $\text{SF}_6$  bubbles of nanometer and micrometer sizes in  $\alpha$ -CD and urea solutions observed by STXM, as shown by the white domains, confined between the two silicon nitride windows. Considering the very strong absorption of water and solid particles, the contrast of the gas

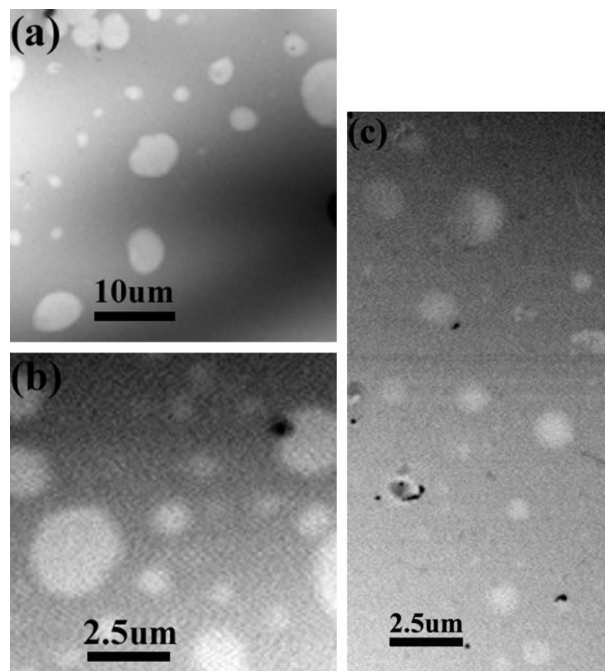


**Figure 3**  
STXM transmission images of (a) Ne nanobubbles at 890 eV in  $\alpha$ -CD (concentration 5  $\text{mg ml}^{-1}$ ), (b)  $\text{SF}_6$  nanobubbles at 697 eV in urea solution (4.5  $\text{mg ml}^{-1}$ ) and (c)  $\text{SF}_6$  nanobubbles in the carbon mesoporous particles solution.

bubbles was white at these energies (Bearden & Burr, 1967). In addition, we used carbon mesoporous particles as gas carriers to bring more  $\text{SF}_6$  gas into the water solution and found a lot of submicroscopic white domains as shown in Fig. 3(c). This means that without organic molecules gas bubbles could also exist stably in a carbon/water system.

In order to confirm that these bubbles did indeed contain gas, we performed a degassing experiment; such a technique has proven to be an important method for distinguishing between gas nanobubbles and possible contaminations in AFM experiments (Zhang *et al.*, 2004). Two degassed experiments were performed. In the first, water was degassed first and then  $\alpha$ -CD, urea or microparticles were added separately. These solutions were measured by STXM to prove that the white domains formed above were not composed of organic molecules, as shown in Fig. 4. In the second degassing experiment, the solutions injected with Ne gas in the urea solutions were degassed for  $\sim 2$  h and then measured by STXM. These degassing experiments both showed that very few bubble-like shapes were observed in those systems containing  $\alpha$ -CD, urea or microparticles. The statistical results clearly proved that bubble-like domains in STXM images were formed by  $\text{SF}_6$  or Ne gas and not from contaminations.

Stability is an important issue in nanobubbles research. The stability of bubbles of different sizes from 100 nm to 20  $\mu\text{m}$  was investigated by taking advantage of the STXM technique which can image small and large bubbles at the same time. It was shown that smaller bubbles were much more stable than larger bubbles. The morphologies of the smaller bubbles did not change much even after scanning 130 times continuously,

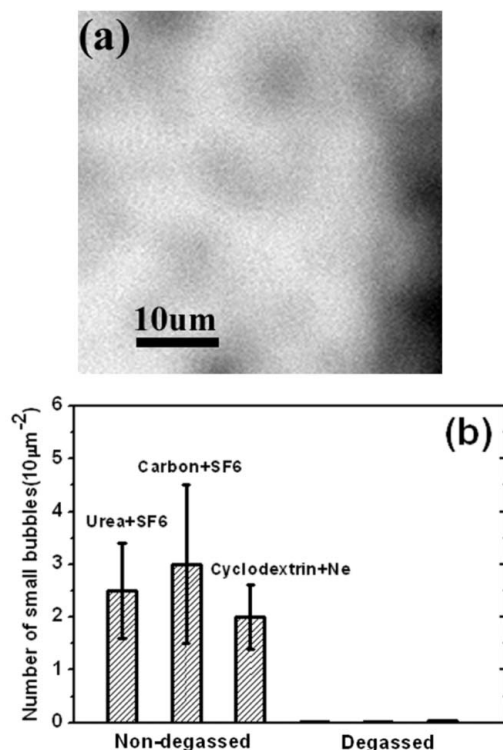


**Figure 4**  
 (a) STXM transmission images of degassed  $\alpha$ -CD solution ( $5 \text{ mg ml}^{-1}$ ) at 695 eV. (b) The effect of degassing on the formation of nanobubbles. The average number of nanobubbles per  $10 \mu\text{m}^2$  clearly decreased when the solutions were degassed.

as shown in Fig. 5. However, larger bubbles were relatively unstable under the soft X-ray irradiation. Fig. 6 shows a typical phenomenon of the growth of large SF<sub>6</sub> bubbles after scanning one, three, five and six times. It can be seen that the large bubble marked in the figures grew larger and larger with increasing scanning times. In addition, further bubbles were produced near this marked bubble.

We analyzed the size distribution of the stable bubbles observed in different solutions and the results are given in Fig. 7. It was found that the lateral (based) diameters of most stable bubbles were usually smaller than  $2.5 \mu\text{m}$ , as shown in Fig. 7(c). There was a slight variation between the different gases: for example, in the SF<sub>6</sub> system the bubble sizes were smaller than those in the Ne system. The phenomenon that the smaller bubbles were more stable than the large bubbles is consistent with the results from the AFM experiments reported in our previous publication that showed that nanobubbles were very stable if their curvature diameters were below  $2.0 \mu\text{m}$  (Zhang *et al.*, 2010). STXM can only provide two-dimensional images of nanobubbles and has no information on the height of the bubbles. However, according to AFM experiments (Zhang *et al.*, 2006, 2010) the lateral sizes of nanobubbles on the solid/water interface could reach the micrometer scale but their heights are less than 100 nm because their contact angles are very low, in the range  $10\text{--}40^\circ$ , on the solid/water interfaces (Craig, 2011). Most of the bubbles in this experiment have lateral sizes below  $1.0 \mu\text{m}$  as

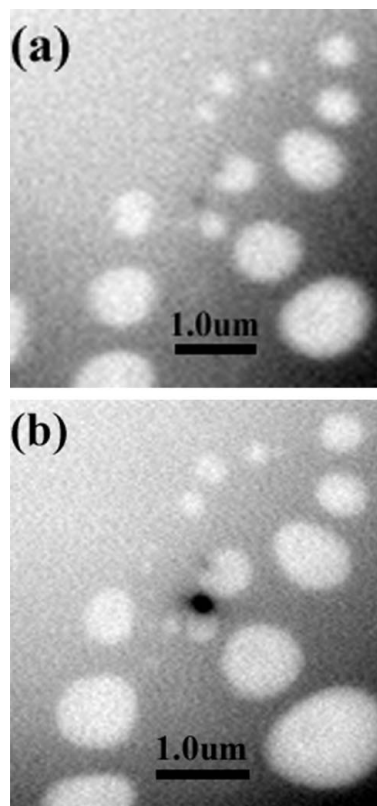


**Figure 5**  
 (a) STXM transmission images of SF<sub>6</sub> nanobubbles and (b) after scanning 130 times.

shown in Fig. 7. We believe that their heights are also less than 100 nm.

Although there was no probe perturbation here, the soft X-rays may have some heating effect on the stability of the gas bubbles. A temperature increase may have a larger effect on the large bubbles than on the smaller bubbles. This phenomenon also proved that the content of these bubble-like domains was gas. Another possible mechanism for the instability of large bubbles is photoionization-induced surface-tension reduction (Weon *et al.*, 2008, 2011); however, these mechanisms need to be proved by systematic experiments in the future.

Since STXM has the ability to provide chemical information about the samples, we attempted to perform absorption spectroscopy near the F *K*-edge energy of SF<sub>6</sub> inside the nanobubbles. Unfortunately, we failed to obtain confident results in terms of the signal-to-noise level in our instrument. The main reason for this may be due to weak absorption of the gas and the current detector not detecting sufficient signals inside the nanobubbles. Further improvements to the STXM technique should be made in the future.

#### 4. Conclusions

We have reported a new STXM technique which could be used to investigate the formation and stability of gas nanobubbles including SF<sub>6</sub> and Ne on Si<sub>3</sub>N<sub>4</sub> surfaces. The experi-

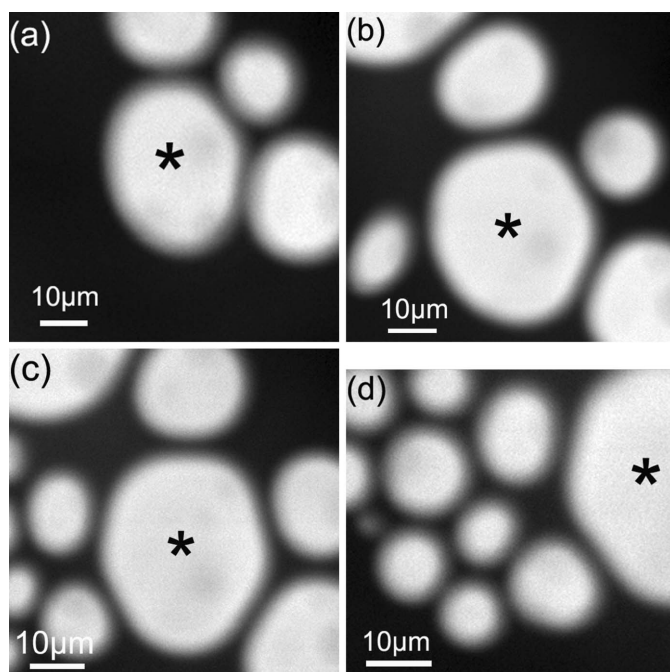


**Figure 6**  
STXM transmission images of microscopic SF<sub>6</sub> bubbles after scanning one (a), three (b), five (c) and six (d) times.

mental results showed that these gas bubbles were stable if their lateral sizes were smaller than 2.5 μm under soft X-ray irradiation. We showed that STXM was a useful tool for investigating individual nanobubbles but more improvements are needed in the future to obtain chemical information inside nanobubbles.

LZ thanks Tolek Tyliczszak (Advanced Light Source, USA) and Jian Wang (Canadian Light Source, Canada) for their kindly discussions on this experiment. This work was supported by the National Science Foundation of China under grant No. 11079050, and the Knowledge Innovation Program of the Chinese Academy of Sciences, No. KJXC2-EW-W09.

## References

- Ball, P. (2012). *ChemPhysChem*, **13**, 2173–2177.  
 Bearden, J. & Burr, A. (1967). *Rev. Mod. Phys.* **39**, 125–142.  
 Borkent, B. M., de Beer, S., Mugele, F. & Lohse, D. (2010). *Langmuir*, **26**, 260–268.  
 Brenner, M. P. & Lohse, D. (2008). *Phys. Rev. Lett.* **101**, 214505.  
 Chao, W., Harteneck, B. D., Liddle, J. A., Anderson, E. H. & Attwood, D. T. (2005). *Nature (London)*, **435**, 1210–1213.  
 Craig, V. S. J. (2011). *Soft Matter*, **7**, 40–48.  
 Doshi, D. A., Watkins, E. B., Israelachvili, J. N. & Majewski, J. (2005). *Proc. Natl Acad. Sci.* **102**, 9458–9462.  
 Ducker, W. A. (2009). *Langmuir*, **25**, 8907–8910.  
 Evans, D., Craig, V. & Senden, T. (2004). *Physica A*, **339**, 101–105.  
 Guan, M., Guo, W., Gao, L., Tang, Y., Hu, J. & Dong, Y. (2012). *ChemPhysChem*, **13**, 2115–2118.  
 Guo, W., Shan, H., Guan, M., Gao, L. H., Liu, M. H. & Dong, Y. M. (2012). *Surf. Sci.* **606**, 1462–1466.  
 Holmberg, M., Kuhle, A., Garnæs, J., Mrch, K. A. & Boisen, A. (2003). *Langmuir*, **19**, 10510–10513.

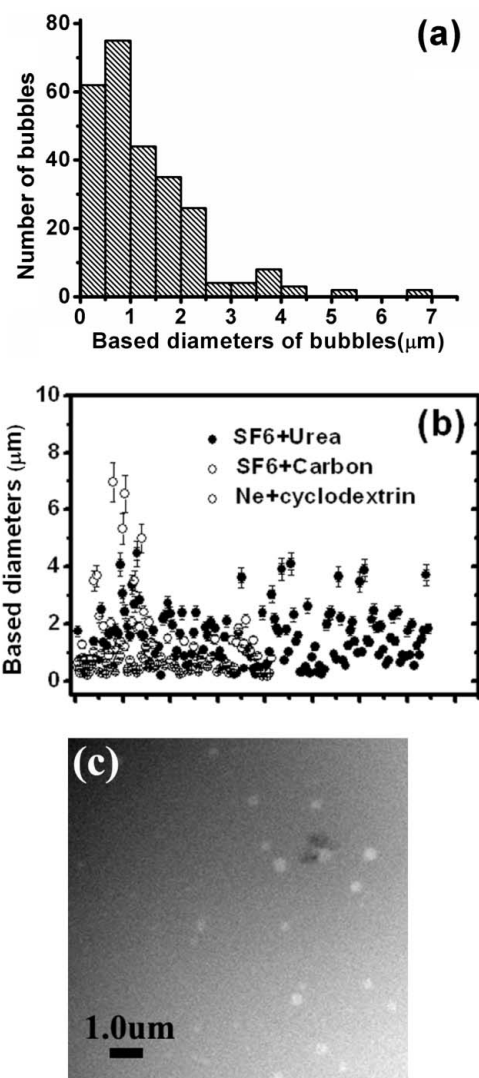


**Figure 7**  
(a) The number of stable bubbles observed by the STXM experiments in α-CD, urea or carbon solution as a function of their diameter. (b) Diameter distribution of the stable bubbles. (c) Typical STXM images of nanobubbles.

- Huang, X., Margulis, C. J. & Berne, B. J. (2003). *Proc. Natl Acad. Sci.* **100**, 11953–11958.  
 Hui, F., Li, B., He, P., Hu, J. & Fang, Y. (2009). *Electrochem. Commun.* **11**, 639–642.  
 Ishida, N., Inoue, T., Miyahara, M. & Higashitani, K. (2000). *Langmuir*, **16**, 6377–6380.  
 Jin, F., Li, J., Ye, X. & Wu, C. (2007). *J. Phys. Chem. B*, **111**, 11745–11749.  
 Karpitschka, S., Dietrich, E., Seddon, J. R., Zandvliet, H. J., Lohse, D. & Riegler, H. (2012). *Phys. Rev. Lett.* **109**, 066102.  
 Liu, P., Huang, X., Zhou, R. & Berne, B. J. (2005). *Nature (London)*, **437**, 159–162.  
 Ljunggren, S. & Eriksson, J. C. (1997). *Colloids Surf. A*, **129/130**, 151–155.  
 Lou, S., Ouyang, Z., Zhang, Y., Li, X., Hu, J., Li, M. & Yang, F. (2000). *J. Vac. Sci. Technol. B*, **18**, 2573.  
 Mezger, M., Reichert, H., Schöder, S., Okasinski, J., Schröder, H., Dosch, H., Palms, D., Ralston, J. & Honkimäki, V. (2006). *Proc. Natl Acad. Sci.* **103**, 18401–18404.  
 Nguyen, A., Evans, G., Nalaskowski, J. & Miller, J. (2004). *Exp. Therm. Fluid Sci.* **28**, 387–394.

- Ohgaki, K., Khanh, N. Q., Joden, Y., Tsuji, A. & Nakagawa, T. (2010). *Chem. Eng. Sci.* **65**, 1296–1300.
- Parker, J. L., Claesson, P. M. & Attard, P. (1994). *J. Phys. Chem.* **98**, 8468–8480.
- Priezjev, N. V., Darhuber, A. A. & Troian, S. M. (2005). *Phys. Rev. E*, **71**, 041608.
- Seddon, J. R., Bliznyuk, O., Kooij, E. S., Poelsema, B., Zandvliet, H. J. & Lohse, D. (2010). *Langmuir*, **26**, 9640–9644.
- Seddon, J. R., Kooij, E. S., Poelsema, B., Zandvliet, H. J. & Lohse, D. (2011). *Phys. Rev. Lett.* **106**, 056101.
- Seddon, J. R. & Zandvliet, H. J. (2010). *Surf. Sci.* **604**, 476–477.
- Seo, H., Yoo, M. & Jeon, S. (2007). *Langmuir*, **23**, 1623–1625.
- Seo, Y. S. & Satija, S. (2006). *Langmuir*, **22**, 7113–7116.
- Simonsen, A. C., Hansen, P. L. & Klösgen, B. (2004). *J. Colloid Interface Sci.* **273**, 291–299.
- Steitz, R., Gutberlet, T., Hauss, T., Klösgen, B., Krastev, R., Schemmel, S., Simonsen, A. C. & Findenegg, G. H. (2003). *Langmuir*, **19**, 2409–2418.
- Vinogradova, O. I. (1995). *Langmuir*, **11**, 2213–2220.
- Wallqvist, A. & Berne, B. J. (1995). *J. Phys. Chem.* **99**, 2893–2899.
- Weon, B. M., Je, J. H., Hwu, Y. & Margaritondo, G. (2008). *Phys. Rev. Lett.* **100**, 217403.
- Weon, B. M., Lee, J. S., Je, J. H. & Fezzaa, K. (2011). *Phys. Rev. E*, **84**, 032601.
- White, E. R., Mecklenburg, M., Singer, S. B., Aloni, S. & Regan, B. C. (2011). *Appl. Phys. Express*, **4**, 055201.
- Wolde, P. R. ten & Chandler, D. (2002). *Proc. Natl Acad. Sci.* **99**, 6539–6543.
- Xue, C., Wang, Y., Guo, Z., Wu, Y., Zhen, X., Chen, M., Chen, J., Xue, S., Peng, Z., Lu, Q. & Tai, R. (2010). *Rev. Sci. Instrum.* **81**, 103502.
- Zhang, L., Zhang, X., Fan, C., Zhang, Y. & Hu, J. (2009). *Langmuir*, **25**, 8860–8864.
- Zhang, L., Zhang, X., Zhang, Y., Hu, J. & Fang, H. (2010). *Soft Matter*, **6**, 4515–4519.
- Zhang, L., Zhang, Y., Zhang, X., Li, Z., Shen, G., Ye, M., Fan, C., Fang, H. & Hu, J. (2006). *Langmuir*, **22**, 8109–8113.
- Zhang, X. H. (2008). *Phys. Chem. Chem. Phys.* **10**, 6842–6848.
- Zhang, X. H., Khan, A. & Ducker, W. A. (2007a). *Phys. Rev. Lett.* **98**, 136101.
- Zhang, X. H., Maeda, N. & Hu, J. (2008b). *J. Phys. Chem. B*, **112**, 13671–13675.
- Zhang, X. H., Quinn, A. & Ducker, W. A. (2008a). *Langmuir*, **24**, 4756–4764.
- Zhang, X. H., Zhang, X. D., Lou, S. T., Zhang, Z. X., Sun, J. L. & Hu, J. (2004). *Langmuir*, **20**, 3813–3815.
- Zhang, X. H., Zhang, X., Sun, J., Zhang, Z., Li, G., Fang, H., Xiao, X., Zeng, X. & Hu, J. (2007b). *Langmuir*, **23**, 1778–1783.